catalysts

MDPI

Article

Photocatalytic Behavior of Strontium Aluminates Co-Doped with Europium and Dysprosium Synthesized by Hydrothermal Reaction in Degradation of Methylene Blue

Byung-Geon Park

Department of Food and Nutrition, Kwangju Women's University, 165 Sanjung-dong, Gwangju 62396, Korea; bgpark@kwu.ac.kr or bgpark814@daum.net; Tel.: +82-62-950-0814

Received: 4 April 2018; Accepted: 22 May 2018; Published: 28 May 2018

Abstract: Strontium aluminates co-doped with europium and dysprosium were prepared by a hydrothermal reaction through a sintering process at lower temperatures. The physicochemical properties of the strontium aluminates co-doped with europium and dysprosium were characterized and compared with those of strontium aluminates prepared by a sol–gel method. The photocatalytic properties of the strontium aluminates co-doped with europium and dysprosium were evaluated through the photocatalytic decomposition of methylene blue dye. The strontium aluminates co-doped with europium and dysprosium prepared by the hydrothermal reaction exhibited good phosphorescence and photocatalytic activities that were similar to those prepared by the sol–gel method. The photocatalytic activity of these catalysts for methylene blue degradation was higher than that of the titanium dioxide (TiO_2) photocatalyst.

Keywords: strontium aluminates; dye photodecomposition; hydrothermal reaction; sol–gel method; phosphorescence

1. Introduction

Alkaline earth aluminates have attracted considerable attention as long afterglow materials because of their excellent photoluminescence, radiation intensity, color purity, and good radiation resistance [1]. In particular, strontium aluminates (SAO) co-doped with europium and dysprosium (SAO; $SrAl_2O_4$: Eu^{2+}, Dy^{3+}) are used in many fields owing to their excellent phosphorescence [2]. $SrAl_2O_4$: Eu^{2+}, Dy^{3+} is applied in emergency lighting, safe indications, signposts, graphic art, billboards, and interior design [3–5]. In addition, the material can be used to synthesize new metal compound composites [6] as well as cathoderay tubes and plasma display panels [7,8]. They also exhibit photocatalytic activity owing to their photosensitive properties [9].

The sol–gel process has attracted considerable interest in obtaining novel chemical compositions and relatively lower reaction temperatures, resulting in homogeneous products [9]. The process enables the synthesis of phosphors with a small size. The inorganic salt-based sol–gel approach has attracted greater interest than the alkoxide-based sol–gel process in the preparation of strontium aluminate luminescent materials [10,11] because inorganic salts are usually non-toxic and cheaper than alkoxides.

Many methods for preparing SAOs have been reported, such as high temperature solid-state reactions [12,13], sol–gel methods [14–16], co-precipitation methods [17], and hydrothermal reaction methods [18,19]. To prepare SAOs by sol–gel method, the mixed reactant sol process should be calcined at temperatures higher than 1000 °C as lower temperatures will not lead to SAOs with good

crystallinity [20]. The calcination temperature should be lowered to accomplish low-cost preparation of SAOs.

This paper reports the preparation of SAOs by a hydrothermal reaction through a sintering process at lower temperatures. The physical properties and phosphorescence of SAOs were characterized and compared with those of SAOs prepared by the sol–gel method. The photocatalytic decomposition of methylene blue (MB) dye using SAO was performed to estimate its photocatalytic activities for the photocatalytic degradation of methylene blue dye.

2. Results and Discussion

2.1. Physicochemical Properties of the SAOs

Figure 1 presents X-ray diffraction (XRD) patterns of the SAOs obtained by a hydrothermal reaction and sol–gel method. Single-phase SAOs were obtained from the two methods. The positions and intensities of the main peaks of the two SAOs corresponded entirely to the standard card (No 34-0379). This suggests that the products were the $SrAl_2O_4$ phase. The XRD patterns of SAOs prepared by hydrothermal reaction showed many reflections. Small quantities of $Sr_3Al_2O_6$ and $SrAl_4O_7$ were observed on the particle surface. Figure 2 presents scanning electron microscopy (SEM) images of the SAOs synthesized by the hydrothermal reaction and sol–gel methods. The SAOs were polycrystalline, and the particles were sintered into irregular shapes due to the high calcination temperature. The crystallinity of SAOs prepared by the sol–gel method was superior to that prepared by the hydrothermal reaction. In particular, SEM images of the SAOs prepared by a hydrothermal reaction showed smaller crystals on the surface of the particles. This suggests that the smaller crystals on the particle surface in the SEM images are the $Sr_3Al_2O_6$ and $SrAl_4O_7$ phases.

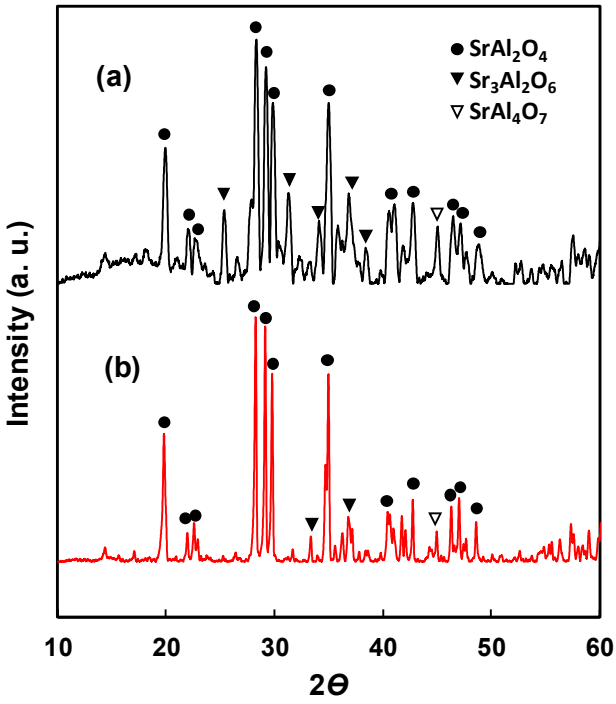

Figure 1. XRD patterns of strontium aluminates (SAO) synthesized by (**a**) hydrothermal reaction and (**b**) sol–gel method.

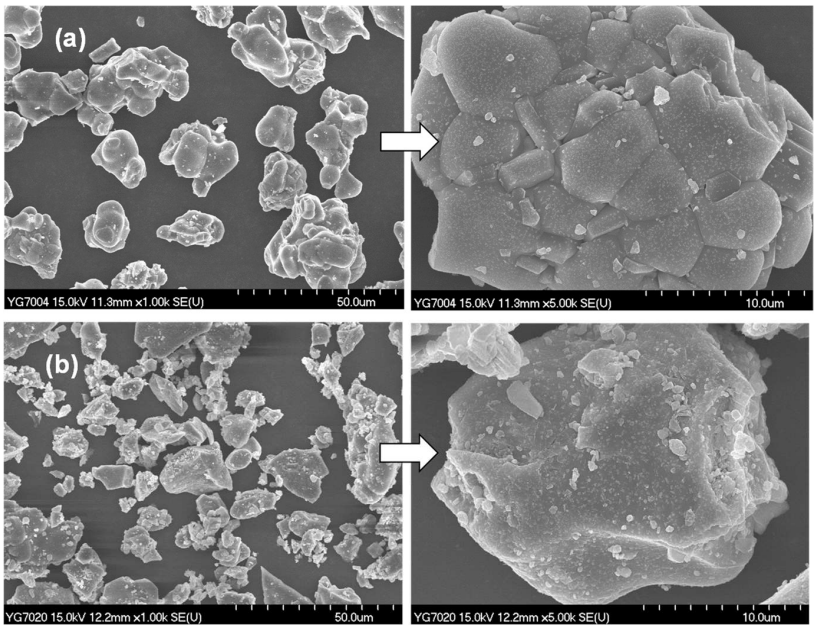

Figure 2. Scanning electron microscopy (SEM) images of SAOs synthesized by (**a**) hydrothermal reaction and (**b**) sol–gel method.

Figure 3 presents the energy-dispersive X-ray (EDX) spectra of the SAOs prepared by the hydrothermal reaction and sol–gel methods. Peaks for Sr and Al were observed. The intensities of the Sr and Al peaks in SAOs prepared by a hydrothermal reaction were similar to those prepared by the sol–gel method. Figure 4 presents Fourier transform infrared (FTIR) spectra of the SAOs. $SrAl_2O_4$ belongs to a distorted stuffed tridymite structure. Tridymite is a member of the nepheline family of structures consisting of a corner-sharing tetrahedral framework that distorts to form large cation-occupying cavities. In $SrAl_2O_4$, the framework is built up by AlO_4 tetrahedra and the structural channels are occupied by Sr^{2+} ions [21]. The XO_4 molecule will have four degenerate normal modes of vibrations: Symmetric stretching (γ_s), symmetric bending (δ_s), antisymmetric stretching (γ_{as}), and antisymmetric bending (δ_d) [22].

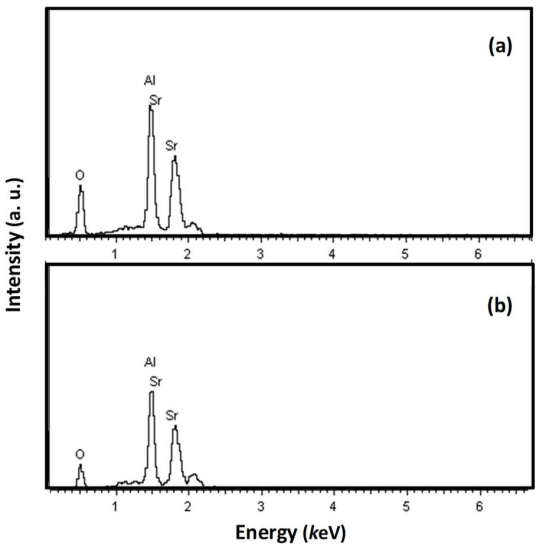

Figure 3. Energy-dispersive X-ray (EDX) spectra of SAOs synthesized by (**a**) hydrothermal reaction and (**b**) sol–gel method.

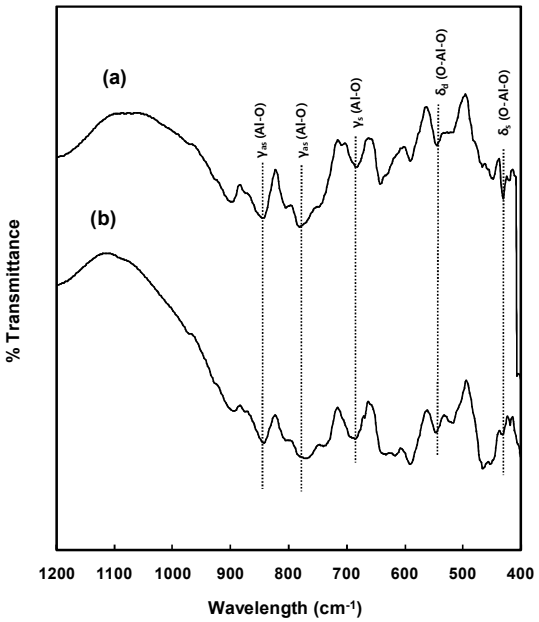

Figure 4. Infrared spectra of the SAOs prepared by (**a**) hydrothermal reaction and (**b**) sol–gel method.

Figure 5 presents the N_2 isotherm of SAOs prepared by a hydrothermal reaction. SAOs are composed of single crystals, as defined in the SEM images. The type of isotherm of SAOs indicated the typical adsorption pattern of nonporous particles. The hysteresis in the isotherm curve was derived from some crevices between the particles. The specific surface areas of the SAOs determined from the Brunauer–Emmett–Teller (BET) equation were 62.5 m^2/g and 51.6 m^2/g, respectively.

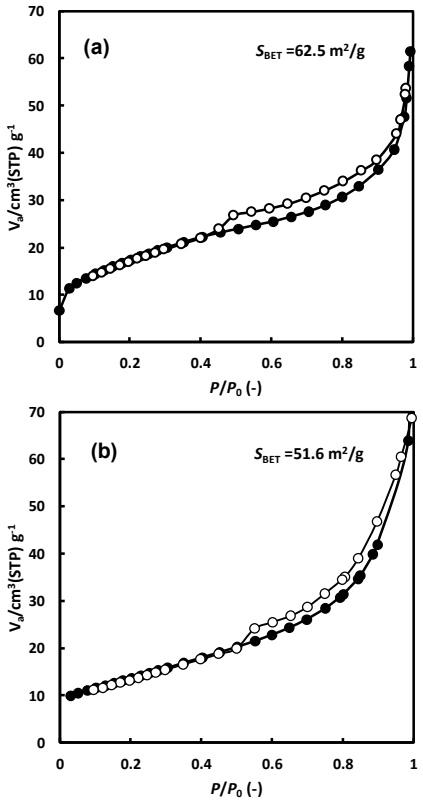

Figure 5. N_2 isotherm of SAOs prepared by (**a**) hydrothermal reaction and (**b**) sol–gel method.

2.2. Luminescent Properties of the SAO Products

Figure 6 presents the emission spectra of the SAOs prepared by the hydrothermal reaction and sol–gel methods. The luminescence properties of the SAO particles were measured in the solid state at room temperature. Regardless of the preparation methods, the SAO particles exhibited similar emission peaks centered at approximately 615 nm under an excitation of 266 nm. The intensities of the peaks for the SAOs prepared by both synthesis methods were similar, which was associated with the typical $4f^6 5d^1 \rightarrow 4f^7$ transition of the Eu^{2+} ion in $SrAl_2O_4$. This strongly affected the nature of the Eu^{2+} surroundings, where the shielding function of the electrons in the inner shell split the mixed states of 4f and 5d by the crystal field [23]. The special emissions of Dy^{3+} and Eu^{3+} were not observed in the spectra. The Eu^{3+} ions in the precursor were reduced to Eu^{2+} in a weak reducing atmosphere. The Eu^{2+} ions in the precursor were reduced to Eu^{+}. The Dy^{3+} ions were oxidized to Dy^{4+} during excitation [24]. Simultaneously, thermal vibrations of the surrounding ions and local vibrations in the lattice structure resulted in luminescence spectra with broad bands [25]. The SAOs prepared by the hydrothermal reaction through lower temperature calcination exhibited a similar emission intensity to the SAOs prepared by the sol–gel method through a higher temperature calcination.

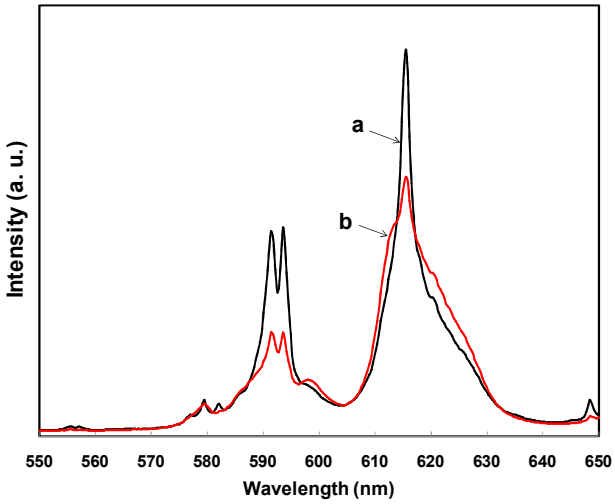

Figure 6. Emission spectra of the SAOs prepared by (**a**) hydrothermal reaction and (**b**) sol–gel method.

Figure 7 presents the UV-visible diffuse reflectance spectra (DRS) results of the SAOs and titanium dioxide (TiO_2) converted to Kubelka–Munk units. The optical bandgap (E_{gap}) was calculated using the method proposed by Kubelka and Munk for indirect electronic transitions [26]. The Kubelka–Munk equation is expressed as $F(R) = (1 - R)^2/2R = K/S$, where R, K, and S are the absolute reflectance, absorption coefficient, and scattering coefficient, respectively. The optical properties of the SAOs were induced by light absorption in the photochemical reaction. The diffuse reflectance spectrum of TiO_2 exhibited an adsorption edge at ca. 380 nm. The bandgap of TiO_2 determined from the adsorption edge was 3.2 eV. By contrast, the DRS of the SAOs were shifted to the upper wavelength range. The SAOs exhibited a significant increase in wavelength. The bandgap of the SAOs was ca. 2.9 eV.

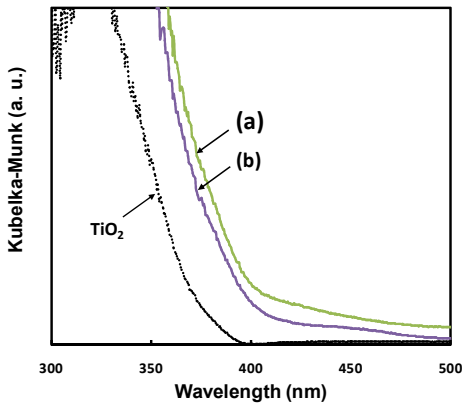

Figure 7. UV-visible diffuse reflectance spectra (DRS) of the SAOs prepared by (**a**) hydrothermal reaction and (**b**) sol–gel method.

2.3. Photocatalytic Properties of the SAO

Figure 8A presents the UV-vis spectra of a pure MB solution, MB solution containing SAO prepared by a hydrothermal reaction, and MB solution containing SAO prepared by the sol–gel method. The absorbance increased with the injection of SAOs prepared by different methods in the MB solution. Figure 8B presents the absorbance of the MB solution containing SAO prepared by hydrothermal reaction and the sol–gel method as a function of the irradiation time of UV light at 300 nm. The absorbance decreased with the injection of SAO into the MB solution despite the short irradiation time. This indicates that the injection of SAOs into the MB solution leads to rapid degradation of the MB dye, and the degradation rate was higher in the MB solution containing SAO prepared by the sol–gel method.

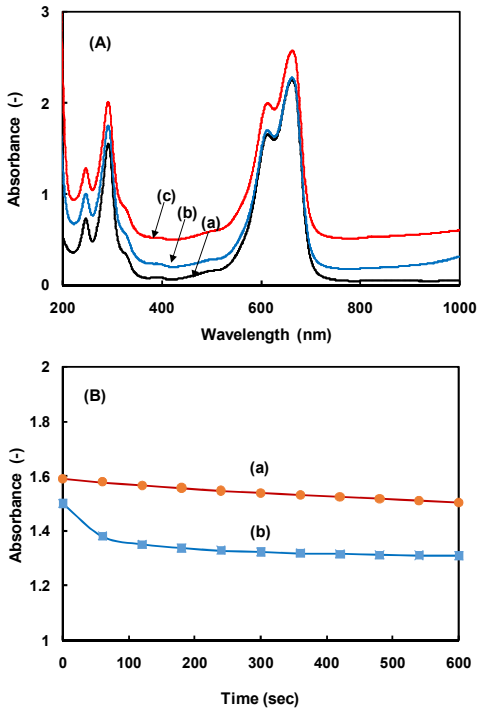

Figure 8. Results of (**A**) UV-vis spectra of as a function of wavelength of (**a**) methylene blue(MB) solution, (**b**) MB solution containing SAO prepared by hydrothermal reaction, and (**c**) MB solution containing SAO prepared by sol–gel method; (**B**) variation of absorbance of the MB solution containing (**a**) SAO prepared by hydrothermal reaction, and (**b**) SAO prepared by sol–gel method as a function of irradiation time of UV light at 300 nm.

Figure 9a presents the changes in MB concentration with different initial MB concentrations on a TiO_2 photocatalyst. The MB concentrations decreased due to the photocatalytic decomposition of MB. The rate of MB degradation was faster at lower initial concentrations of MB than at higher initial concentrations because the photoefficiency increases with decreasing dye concentration. In addition, a large amount of dye might be adsorbed on the TiO_2 surface, which can prevent the dye molecules from coming in contact with the free radicals and electron holes. Figure 9b shows the photocatalytic degradation of MB on TiO_2 and the SAO photocatalysts at the same initial concentration of MB. The degradation of MB was faster with the SAO photocatalysts than that with the TiO_2 photocatalyst. This suggests that SAOs have higher photocatalytic activity than the TiO_2 photocatalyst. The higher photocatalytic activity of SAO was attributed to its higher photosensitivity, which was defined in the DRS results. The SAOs showed a lower bandgap than TiO_2. A lower bandgap of SAOs led to enhanced photocatalytic activity than TiO_2.

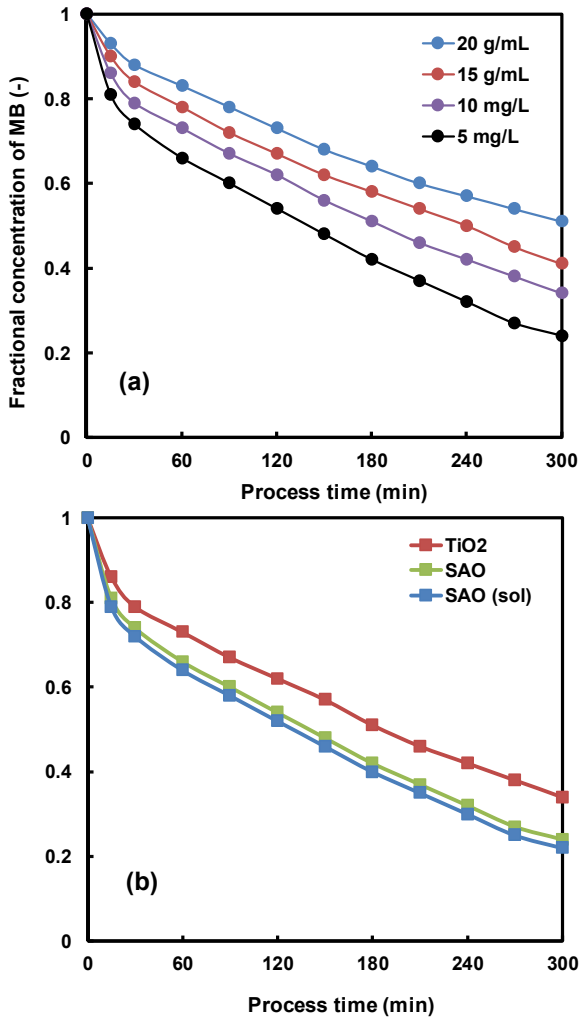

Figure 9. Variation of the concentration of MB by the photocatalytic decomposition on titanium dioxide (TiO_2) with (**a**) various initial concentrations and (**b**) on SAOs at an initial MB concentration of 10 mg/L.

3. Materials and Method

3.1. Preparation of SAOs

The SAOs were prepared by both a sol–gel method and hydrothermal reaction. In both methods, aluminum nitrate nonahydrate ($Al(NO_3)_3 \cdot 9H_2O$, 99%; Duksan, Ansan-City, Korea), strontium nitrate

($Sr(NO_3)_3$,99%; Duksan, Ansan-City, Korea), dysprosium(III) nitrate pentahydrate ($Dy(NO_3)_3 \cdot 5H_2O$, 99%; Alfa Aesar, Ward Hill, MA, USA), and europium(III) nitrate hexahydrate ($Eu(NO_3)_3 \cdot 6H_2O$, 99%; Alfa Aesar, Ward Hill, MA, USA) were dissolved in distilled water with stirring for 30 min at 90 °C. The chemicals of the reactants were of analytical grade and used as received. The solutions were combined according to the molar ratio of Sr:Al:Eu:Dy = 0.97:2:0.01:0.02.

The chelating reagent solution was prepared using the appropriate amount of aqueous citric acid solution and added dropwise to the above solution. A boric acid solution was then added to the chelating reagent solution. The mixture was concentrated at 80 °C with stirring until it changed to a high viscosity translucent gel. The mixture was then calcined in an electric muffle furnace at 1100 °C for 3 h in a weak reducing atmosphere using a hydrogen-containing gas mixture ($Ar:H_2$ = 95:5).

SAOs were also prepared by a hydrothermal reaction. The mixture of SAO precursors and the chelating agent solution were poured in an autoclave. The autoclave containing the reactant was heated to 130 °C with stirring using a magnetic stirrer. The hydrothermal reaction conditions were maintained for 5 h. After the hydrothermal reaction, the product was dried at 110 °C for 12 h. The product was then calcined at 550 °C for 4 h in a reducing atmosphere. Commercially available TiO_2 (Degussa, P25, Krefeld, Germany) with a particle size and specific area of ≈30 nm and ≈50 m^2/g, respectively, was also used for photocatalytic decomposition.

3.2. Photocatalytic Decomposition of Methylene Blue

The MB solution (100 mL) was mixed with the photocatalysts as a reactant mixture. The photocatalyst loading was adjusted to 5 mL because of the significant difference in the densities between TiO_2 and SAOs. The reactant mixture was stirred in the dark for 1 h to reach adsorption equilibrium. The reactant mixture was irradiated with UV light with stirring. Samples were taken at regular intervals. They were the centrifuged and the photocatalysts were separated. The concentrations of the samples were analyzed by UV-visible spectrophotometry (Shimadzu UV-2450, Tokyo, Japan). The concentrations of MB were determined from the calibrated absorbance at 665 nm using a spectrophotometer.

The photocatalytic degradation of MB was carried out using a glass reactor-installed UV lamp system. The reactor was kept in the dark to prevent the dispersion of UV light during the photoreaction. The photoreaction temperature was maintained at 25 °C. The UV array consisted of two 10 W UV-A lamps. The UV emission wavelength and light strength was 365 nm and 30 Lx, respectively.

3.3. Characterization of the SAOs

The phase of the SAO particles was determined by XRD (Rigaku Model D/max-II B, Texas, USA). XRD was conducted at 40 kV and 30 mA with a scan speed of 5°/min, scanning angle from 10° to 60°, and a step of 0.02° using Cu Kα radiation. The crystal size and morphology of the SAOs were investigated by SEM (Hitachi S-4700, Tokyo, Japan). Their chemical components were analyzed by EDX (NORAN Z-MAX 300 series, Tokyo, Japan). The N_2 isotherms of the SAOs were investigated using a volumetric adsorption apparatus (Mirae SI, Porosity-X, Gwangju, Korea) at liquid N_2 temperature. The sample was pretreated at 150 °C for 1 h before exposure to nitrogen gas. The surface areas of the samples were calculated using the BET equation [27]. Transmission electron microscopy (TEM, JEOL JEM-2100F, Tokyo, Japan) was performed using a LaB_6 filament and operated at 200 kV.

The composition of the phosphors was analyzed using an EDX micro analyzer (JEOL JSM-840A, Tokyo, Japan) mounted on the microscope. The photoluminescence was evaluated by photoluminescence spectroscopy (PL, Spectrograph 500i, Acton Research Co., Acton, MA, USA) with a 0.2 nm resolution at room temperature. The samples were excited at 226 nm using a He-Cd laser. The UV–vis diffuse reflectance spectra were measured using a UV-vis spectrometer (Shimadzu UV-2450, Tokyo, Japan) in the region, 200–700 nm, with $BaSO_4$ as the reflectance standard. The optical bandgap (E_{gap}) was calculated using the Kubelka–Munk method for indirect electronic transitions.

4. Conclusions

Strontium aluminates co-doped with europium and dysprosium was prepared by a hydrothermal reaction through a sintering process at lower temperatures. The physicochemical properties of the SAOs characterized by SEM-EDX, photoluminescence, and UV-visible DRS were similar to those of the SAOs prepared by the sol–gel method. Although SAOs had been calcined at lower temperatures, their characteristics matched the standard. The photocatalytic activity for the photodecomposition of MB dye was higher than that of the TiO_2 photocatalyst. The SAOs exhibited higher photocatalytic activity than the TiO_2 photocatalyst. The higher photocatalytic activity of SAO was attributed to its higher photosensitivity.

Acknowledgments: This paper was supported by Research Funds of Kwangju Women's University in 2017.

Conflicts of Interest: The author declares no conflict of interest.

References

1. Du, H.; Shan, W.; Wang, L.; Xu, D.; Yin, H.; Chen, Y.; Guo, D. Optimization and complexing agent-assisted synthesis of green $SrAl_2O_4$: Eu^{2+}, Dy^{3+} phosphors through sol-gel process. *J. Lumin.* **2016**, *176*, 272–277. [CrossRef]
2. Amato, C.A.; Giovannetti, R.; Zannotti, M.; Rommozzi, E.; Ferraro, S.; Seghetti, C.; Minicucci, M.; Gunnella, R.; Di Cicco, A. Enhancement of visible-light photoactivity by polypropylene coated plasmonic Au/TiO_2 for dye degradation in water solution. *Appl. Surf. Sci.* **2018**, *441*, 575–587. [CrossRef]
3. Katsumata, T.; Nabae, T.; Sasajima, K.; Matsuzawa, T. Growth and characteristics of long persistent $SrAl_2O_4$- and $CaAl_2O_4$-based phosphor crystals by a floating zone technique. *J. Cryst. Growth* **1988**, *183*, 361–365. [CrossRef]
4. Nakamura, T.; Kaiya, K.; Takahashi, N.; Matsuzawa, T.; Rowlands, C.C.; Beltran-Lopez, V.; Smith, G.M.; Riedi, P.C. High frequency EPR of europium(II)-doped strontium aluminate phosphors. *J. Mater. Chem.* **2000**, *10*, 2566–2569. [CrossRef]
5. Lin, Y.; Tang, Z.; Zhang, Z. Preparation of long-afterglow $Sr_4Al_{14}O_{25}$-based luminescent material and its optical properties. *Mater. Lett.* **2011**, *51*, 14–18. [CrossRef]
6. Singh, T.S.; Mitra, S. Fluorescence behavior of intramolecular charge transfer state in *trans*-ethyl *p*-(dimethylamino) cinamate. *J. Lumin.* **2007**, *127*, 508–514. [CrossRef]
7. Kubota, S.; Yamane, H.; Shimada, M. A new luminescent material, $Sr_3Al_{10}SiO_{20}$:Tb^{3+}. *Chem. Mater.* **2002**, *14*, 4015–4016. [CrossRef]
8. Lin, C.C.; Xiao, Z.R.; Guo, G.-Y.; Chan, T.-S.; Liu, R.-S. Versatile phosphate phosphors $ABPO_4$ in white light-emitting diodes: Collocated characteristic analysis and theoretical calculations. *J. Am. Chem. Soc.* **2010**, *132*, 3020–3028. [CrossRef] [PubMed]
9. Kiss, B.; Manning, T.D.; Hesp, D.; Didor, C.; Taylor, A.; Pickup, D.M.; Chadwick, A.V.; Allison, H.E.; Dhanak, V.R.; Claridge, J.B.; et al. Nano-structured rodium doped $SrTiO_3$-visible light activated photocatalyst for water decomposition. *Appl. Catal. B Environ.* **2017**, *200*, 547–555. [CrossRef]
10. Liyuan, X.; Qin, X.; Yingliang, L. Preparation and characterization of flower-like $SrAl_2O_4$: Eu^{2+}, Dy^{3+} phosphors by sol-gel process. *J. Rare Earths* **2011**, *29*, 39–43.
11. Chai, Y.S.; Zhang, P.; Zheng, Z.T. Eu^{2+} and Dy^{3+} co-doped $Sr_3Al_2O_6$ red long-afterglow phosphors with new flower-like morphology. *Phys. B Condens. Matter* **2008**, *403*, 4120–4122.
12. Suriyamurthy, N.; Panigrahi, B.S. Effects of non-stoichiometry and substitution on photoluminescence and afterglow luminescence of $Sr_4Al_{14}O_{25}$: Eu^{2+}, Dy^{3+} phosphor. *J. Lumin.* **2008**, *128*, 1809–1814. [CrossRef]
13. He, Z.; Wang, X.; Yen, W.M. Investigation on charging processes and phosphorescent efficiency of $SrAl_2O_4$: Eu, Dy. *J. Lumin.* **2006**, *119–120*, 309–313. [CrossRef]
14. Ayari, M.; Paul-Boncour, V.; Lamloumi, J.; Mathlouthi, H.; Percheron-Guégan, A. Study of the structural, thermodynamic and electrochemical properties of $LaNi_{3.55}Mn_{0.4}Al_{0.3}(Co_{1-x}Fe_x)_{0.75}$ ($0 \leq x \leq 1$) compounds used as negative electrode in Ni-MH batteries. *J. Alloy. Compd.* **2006**, *420*, 251–255. [CrossRef]
15. Peng, T.; Huajun, L.; Yang, H.; Yan, C. Synthesis of $SrAl_2O_4$: Eu, Dy phosphor nanometer powders by sol–gel processes and its optical properties. *Mater. Chem. Phys.* **2004**, *85*, 68–72. [CrossRef]

16. Cordoncillo, E.; Julian-Lopez, B.; Martínez, M.; Sanjuán, M.L.; Escribano, P. New insights in the structure–luminescence relationship of Eu:$SrAl_2O_4$. *J. Alloy. Compd.* **2009**, *484*, 693–697. [CrossRef]
17. Rezende, M.V.; Montes, P.J.; Soares, F.M.; Santos, C.; Valerio, M.E. Influence of co-dopant in the europium reduction in $SrAl_2O_4$ host. *J. Synchrotron Radiat.* **2014**, *21*, 143–148. [CrossRef] [PubMed]
18. Tao, J.; Pan, H.; Zhai, H.; Wang, J.; Li, L.; Wu, J.; Jiang, W.; Xu, X.; Tang, R. Controls of tricalcium phosphate single-crystal formation from its amorphous precursor by interfacial energy. *Cryst. Growth Des.* **2009**, *9*, 3154–3160. [CrossRef]
19. Zhang, R.; Han, G.; Zhang, L.; Yan, B. Gel combustion synthesis and luminescence properties of nanoparticles of monoclinic $SrAl_2O_4$:Eu^{2+}, Dy^{3+}. *Mater. Chem. Phys.* **2009**, *113*, 255–259. [CrossRef]
20. Peng, T.; Yang, H.; Pu, X.; Hu, B.; Jiang, Z.; Yan, C. Combustion synthesis and photoluminescence of $SrAl_2O_4$:Eu,Dy phosphor nanoparticles. *Mater. Lett.* **2004**, *58*, 352–356. [CrossRef]
21. Megaw, H.D. *Crystal Structure: A Working Approach*; Saunders, W.B.: London, UK, 1973.
22. Nakamoto, K. *Infrared Spectra of Inorganic and Coordination Compounds*; Wiely: London, UK, 1963.
23. Shan, W.; Wu, L.; Tao, N.; Chen, Y.; Guo, D. Optimization method for green $SrAl_2O_4$: Eu^{2+}, Dy^{3+} phosphors synthesized via co-precipitation route assisted by microwave irradiation using orthogonal experimental design. *Ceram. Int.* **2015**, *41*, 15034–15040. [CrossRef]
24. Hong, G.Y.; Jeon, B.S.; Yoo, Y.K.; Yoo, J.S. Photoluminescence characteristics of spherical Y_2O_3: Eu phosphors by aerosol pyrolysis. *J. Electrochem. Soc.* **2001**, *148*, H161–H166. [CrossRef]
25. Xiao, Q.; Xiao, L.; Liu, Y.; Chen, X.; Li, Y. Synthesis and luminescence properties of needle-like $SrAl_2O_4$: Eu, Dy phosphor via a hydrothermal co-precipitation method. *J. Phys. Chem. Solids* **2010**, *71*, 1026–1030. [CrossRef]
26. Kubelka, P.; Munk, F. Ein beitrag zur optik der farbanstriche. *Z. Tech. Phys.* **1931**, *12*, 593–598.
27. Brunauer, S.; Emmett, P.H.; Teller, E. Adsorption of gases in multimolecular layers. *J. Am. Chem. Soc.* **1938**, *60*, 309–319. [CrossRef]